Correlation Study: Triggering and Magnitude of Earthquakes in Italy (≥M4.3) in Relation to the Positions and Gravitational Forces of the Sun, Moon, and Planets Relative to Earth.

Research Proposal · March 2024

DOI: 10.13140/RG.2.2.19714.08646

CITATIONS
0

READS
68

1 author:

Stefano Calandra
EqForecast srl

17 PUBLICATIONS **0** CITATIONS

SEE PROFILE

Correlation Study: Triggering and Magnitude of Earthquakes in Italy (≥M4.3) in Relation to the Positions and Gravitational Forces of the Sun, Moon, and Planets Relative to Earth.

Stefano Calandra: CEO, EqForecast, an innovative start-up in the field of seismic forecasting, Venice, Italy; info@earthquakesforecast.com

Daniele Teti: Physicist, Senior IT, and Researcher, EqForecast, L'Aquila, Italy; info@earthquakesforecast.com

Corresponding author: Stefano Calandra

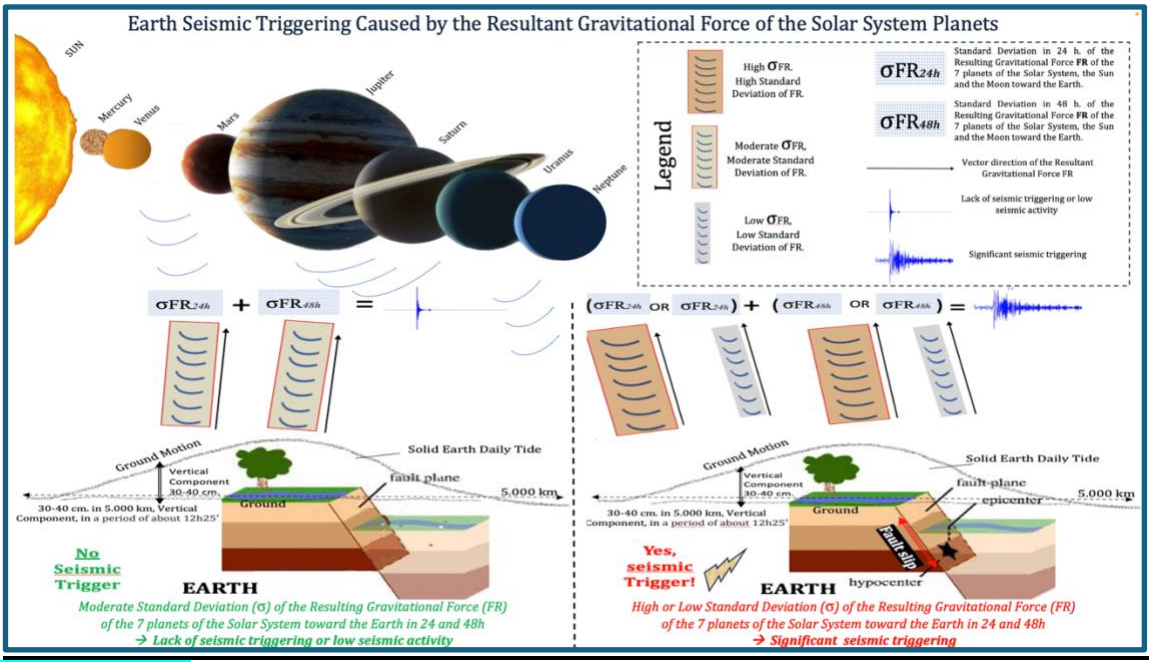

Graphical abstract

Abstract

When earthquakes occur, researchers explore potential correlations between specific gravitational forces and the positions of Solar System planets related to seismic activity. Studies from various times and places have investigated these correlations, including the effects of Solar and Lunar tides, occasionally yielding controversial results. Recent research underscores how Lunar-Solar tides affect the Earth's crust, creating multidimensional oscillations, establishing a link with seismic activity. This study, based on a sample of 200 Italian earthquakes M>4.3 from 1600 to 2022, reveals statistical correlations between the positions of celestial bodies in the Solar System and earthquake magnitudes at the time of earthquake triggering (Hypothesis 1). Additionally, a recurring pattern emerges in the gravitational forces exerted by these celestial bodies during earthquake triggers (Hypothesis 2). These findings suggest that the Lunar-Solar system is not the sole external gravitational factor influencing earthquakes: instead, the "7 Planet System" shows a more significant causal relationship in this context. We utilize an indirect calculation method that involves vector physics and considers the angles formed between pairs of planets and the Earth. The utilization of this data has the potential to contribute to a plausible predictive earthquake model.

Keywords

Earthquake forecasting and prediction; planetary masses; celestial bodies; non-random statistical correlation; gravitational forces; seismic triggers; vertical tidal forces; astro-seismology; early warning systems

1 Introduction

1.1 . A new approach

In this preliminary study, we propose a new approach to investigating the relationship between celestial bodies and earthquakes. We focus on two key aspects: whether the masses of seven Solar System planets, the Moon, and the Sun influence earthquake triggering and magnitude. This study extends the methodology of prior earthquake prediction research, which focused on planetary positions and masses to elucidate earthquake causation (see *infra*, Section 1.3). Nevertheless, these earlier studies did not compute gravitational forces during seismic events to establish direct correlations.

In general, the term *"earthquake prediction"* has been used cautiously and mainly associated with basic research, rather than applied fields. There is only one case [1] in China, where the official support of earthquake prediction research is mentioned, with China intending to study correlations between celestial body positions in the Solar System and earthquakes during the late 1960s and 1970s.

1.2. Non-planetary precursors of strong earthquakes

Researchers have explored *various non-planetary precursors of strong earthquakes*, including electromagnetic fields [2] [3] sonic and neutron emissions [4] solar activity [5], [6] and more recently, an Italian study [7], geographical and abnormal oscillations in latitude and longitude values of precursor earthquakes [8], radon [9] [10] and the Global Positioning System GPS [11] [12].

1.3. Planetary action capable of triggering earthquakes

This study analyzes the potential link between celestial bodies and earthquakes, focusing on the planets, the Moon and the Sun and *basically following the first line of research* (see *infra*, section 1.3.1). Historical research also examines correlations between the positions of celestial bodies and earthquakes and the tidal effects of the Sun and Moon. A study in particular of the second line of research (see *infra*, section 1.3.2) will be taken as the basis of this research.

1.3.1. First line of research

The first line of studies, though less prominent, examines the statistical correlation between the positions of the Sun, Moon phases, planets of the Solar System, and earthquakes. It discusses this connection in relation to directly measuring planet positions. One reason for its relatively lesser attention, particularly among Western researchers, is the scarcity of measurement instruments in the field (see *supra*, Section 1.2).

Dating back to Plinius Secundus (Italy, 23-79 A.D.), the oldest citation in this context associates earthquakes with alignments and quadratures of the Sun with Mars, Jupiter, and Saturn. Plinius states: *"Babyloniorum placita et motus terrae hiatusque, qua cetera omnia, siderum vi existimant fieri, sed illorum trium, quibus fulmina adsignant, fieri autem meantium cum sole aut congruentium et maxime circa quadrata mundi".* "The Babylonian scientific traditions maintain that even the motions and fractures of the Earth, like all other things, occur due to the force of the planets, in particular those three, to which they assign lightning, but they occur in particular when they revolve with the Sun or are in conjunction and especially around quadratures (90°)" [13].

More recently, earthquakes show a heightened occurrence during phases such as Full and New Moons [4], [14], [15], [16] and even Last Quarter and New Moons [17]. Recent work [18], directly connects earthquake-triggering to gravitational forces arising from the interactions between planets, the Sun, Moon, and Earth's tectonic plates.

An emerging trend in India also examines the Sun, Moon, and planets in relation to Earth. This involves categorizing planets into groups to measure their angles during seismic events [19] or calculating angular vectors of gravitational forces from planetary masses to identify earthquake triggers [20].

1.3.2. Second line of study and its significance

Research from the late 1800s explores [21], [22], whether solid tidal forces from the Sun and Moon trigger earthquakes. Correlations between tidal action and earthquakes are supported by evidence and are well-accepted. Recent findings [23], [24] highlight the impact of tides on the solid Earth and crust, or causing multidimensional oscillations during lunar and solar passages [25], [26], [22], [23], [24], [27]. These deformations, combined with plate motion and Earth tide components, link tides to seismic activity.

2. Materials and methods

This study examines 200 earthquakes with a magnitude greater than M4.3 from the ASMI-INGV database [28]. Fifty-five earthquakes were handpicked, while 145 were randomly selected from Italy's 1,590 M4.3+ earthquakes spanning from the 1600s to 2022 (see *infra*, Section 2.10, Table 4).

The Italian study (Zaccagnino et al. 2020) belonging to the second line of research emphasizes the impact of tides on the solid Earth and crust, contributing to seismic activity. Gravitational forces, including the vertical component of tides, can trigger seismicity over time. The vertical component of lunar-solar tides, solid and liquid, can trigger seismicity after decades or centuries, when horizontal energy accumulates.

Following this hypothesis, but due to the lack of instruments on the ground to measure gravitational variations, this study employs indirect computational methods involving vector physics and the angles formed by pairs of planets with Earth (see *infra*, Section 2.8).

Building on the vector approach of the Indian article (Jeganathan, C. et al. 2015) belonging to the first line of research, this study seeks to provide new evidence to support the hypothesis that the forces responsible for triggering earthquakes adhere to Newton's law of universal gravitation.

Historically, links have been established between planetary positions and earthquakes, *but a systematic analysis is missing.* Fortunately, modern computational tools, accessible to individual researchers, have made such studies independent of complex ground surveying technology. State-of-the-art software, relying on Kepler's astronomical laws from 1627, calculates planetary positions, streamlining our calculations. The next section delves into the calculation methods used to input planetary positions related to earthquakes.

2.1. Altazimuth coordinate system

To capture these rapid angular changes of the planets, instead of using one of the other two systems - the equatorial coordinates [20], [22] and the ecliptic coordinates [19] - generally used in the other studies*, we employed altazimuth coordinates*—a reference system tied to the Observer's position shifting with Earth's rotation and Planets' motion. We also extend the use of altazimuth coordinates to showcase the Hypothesis 2 underscoring *the novelty of this astronomical coordinate model in earthquake research.*

This dynamic approach, adjusting with Earth's rotation and planetary movements, enhances sensitivity in calculating planet/earthquake angular correlations. We also extend the use of altazimuth coordinates to showcase the Hypothesis 2 underscoring *the novelty of this astronomical coordinate model in earthquake research.*

2.2. Geographical reference quadrant

A significant challenge was determining how to calculate planetary angles from an Earth observation point. We employed azimuth and elevation coordinates from the Astronomical Tables of VSOP87 [29] to derive the relevant angles for each planet pair. Our Earth observation point aligns with Lat. 42.7°/42.8° and Long. 13.23°, roughly corresponding to Accumoli (RI), Central Italy. The quadrant's bounds are set by the 200 earthquakes analyzed, spanning Lat. 47.18°, Long. 06.80° to Lat. 36.66°, Long. 18.68° including part of the Balkan Peninsula.

2.3. Angular distance of celestial bodies

Accurately determining the angular position of a planet pair relative to Earth involves accounting for *delta elevation* and *delta azimuth*. Representing a three-star system— O =Earth, B=Planet 1, and D=Planet 2—on a Cartesian plane establishes an angular reference system. The angular *value BD serves as the "angular distance",* summarizing the delta between the azimuths and elevations of the 2 planets B and D relative to the Earth observer (figure. 1)

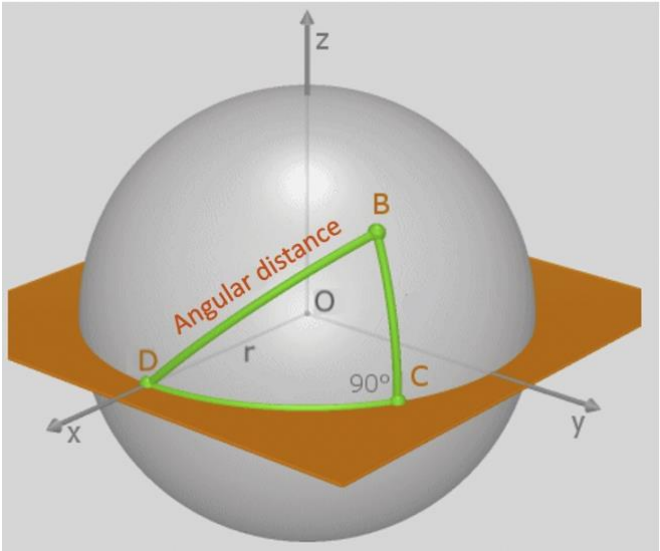

Figure 1. Determination of angular distance in a spherical plane. The angular *value BD serves as the "angular distance",* summarizing the delta between the azimuths DC and the delta between the elevations BC of the 2 planets B and D relative to the Earth O observer. The equation $DB^2 = DC^2 + BC^2$ applicable to the Cartesian plane is adaptable to spherical planes, which are utilized when calculating sidereal distances. However, points B, C, and D lie *on different spherical planes* due to their construction, necessitating simplification if placed on a single spherical plane. The spherical right triangle Pythagorean Theorem converges to the Cartesian plane's classical Pythagorean Theorem when the sphere's radius $r \rightarrow \infty$, we use the Taylor polynomial $1-x2/2$. *This allows us to simplify the "angular distance" from the spherical plane to the Cartesian plane for calculations.*

2.4. Spherical and Cartesian planes

Considering distances between point O in space and points B, C, D (i.e., the sphere's radius r - Figure 1), which can be millions of kilometers apart (e.g., Earth-Jupiter distance $\approx 7.858\times10^8$ km), we can approximate the equation $\cos(DB/r) = \cos(DC/r)\cos(CB/r)$ as if we were in the neighborhood of $\cos(x/r) = 0$, with $r \rightarrow \infty$, using *the Taylor polynomial* $1-x^2/2$.

Subtracting 1 and multiplying by $-2\ R^2$: $DB^2 \approx BC^2 + DC^2 - DC^2\ BC^2/(2r^2)$. As r tends to infinity, the term $DC^2\ BC^2/(2\ r^2)$ tends to zero, making the approximation tend to the exact equality: $\boldsymbol{DB^2 = DC^2 + BC^2}$.

2.5. Hypothesis 1

The Hypothesis 1 follows the first line of research (see *supra*, Section 1.3.1) and posits that earthquakes with magnitudes ≥M4.3 are connected to the conjunctions and oppositions of the seven planets of the Solar System, along with the Moon and the Sun in relation to Earth. To substantiate this, we aim to illustrate that *specific angular distances DB* of these celestial bodies, as observed from the earthquake's epicenter, correlate with earthquake magnitudes within short observation periods: usually hours instead of weeks or months.

Within 48 hours of an earthquake, we consistently monitored the positions of the seven Solar System planets, the Moon, and the Sun relative to the observer on Earth. We found that a meaningful statistical

correlation emerges when the number of precise planet pair conjunctions or oppositions with Earth increases, resulting in higher average earthquake magnitudes (see infra, Section Results, 3.1).

2.6. Developing the Hypothesis 1 method

Empirical evidence indicates that when we examine the angular distance BD (Fig. 2) between the seven planets of the Solar System (excluding Pluto), the Moon, and the Sun in pairs, relative to an observer on Earth within the earthquake's epicenter's geographic area, *values approaching 0°, within a fixed BD tolerance of 0° -/+12°, become significant indicators of earthquake magnitudes.*

This value corresponds to n(n-1)/2 = 36 unique combinations of angle pairs formed by the 9 celestial bodies relative to Earth. The analysis proceeds graphically with software deriving values from astronomical tables, particularly the "angular distance" between celestial bodies observed from Earth. See Table 1 for software configuration. Data processing is facilitated by dedicated software named VS0P87 - Celestial Sphere - Delta. The software utilizes astronomical data and processes it according to the described method, providing the necessary values.

Table 1 DOI 10.5281/zenodo.7746082, VSOP87 - Celestial Sphere - Delta Mask and Software, for Section 2.6

Aggregate results are presented in Results (see *infra*, Section 3.1).

2.7. Hypothesis 2

We discuss the role of *resultant gravitational forces (henceforth "FR")* as a vertical tidal force (see *supra*, Section 2 and *infra*, Discussion, 4.4) component affecting seismic activity.

The Hypothesis 2 suggests that the primary factor influencing seismic triggering isn't the absolute magnitude of FR from the lunar-solar system and Solar System planets. Instead, it's the *stability/unstability fluctuations of FR within 24-48 hours of an earthquake that matter most.* We assess these fluctuations through change values or *standard deviations of FR (henceforth "*σFR*)*, introducing a *novel aspect to existing researches.*

Experimental evidence shows a stronger link between seismic activity and the Solar System's seven planets σFR, surpassing the Luni-Solar system's influence (see *infra*, Section 3.1.1). Testing the hypothesis indirectly measures FR by observing the angles (see *supra*, Section 2.3) formed by planets concerning an earthquake's epicenter. These findings are relevant *over hours* rather than extended astronomical observations.

2.8. Developing the Hypothesis 2 method

To examine the Hypothesis 2, we turn to vector physics. This involves creating vectors for all the FR generated by the planets to Earth and measuring their values. *The FR expressed in Newton's results from the sum of the product of the two force vectors, each multiplied by the cosine of the adjacent angles.* This theory is grounded in Newton's Law of Universal Gravitation [30].

Also this data processing is facilitated by dedicated software named VS0P87 - Celestial Sphere - Delta. The software utilizes astronomical data and processes it according to the described method, providing the necessary values. By appropriately entering the date and other data, see the URL of the data setting mask that enables the calculation of the resultant gravitational force FR, in Table 2.

Table 2 DOI 10.5281/zenodo.7734562, VSOP87 - Celestial Sphere - Delta Mask and Software, for Section 2.8.

In the context of this study, where the number of FR to be measured at each time "t" exceeds two vectors, it is more convenient *to represent these vectors in coordinates* and then simply add them component by component. Practically speaking, for each of the n=9 celestial bodies – Sun, Moon,

Mercury, Venus, Mars, Jupiter, Saturn, Uranus, Neptune – we calculate the resulting gravitational force vector exerted during the Astro/Earth interaction at every instant to Earth.

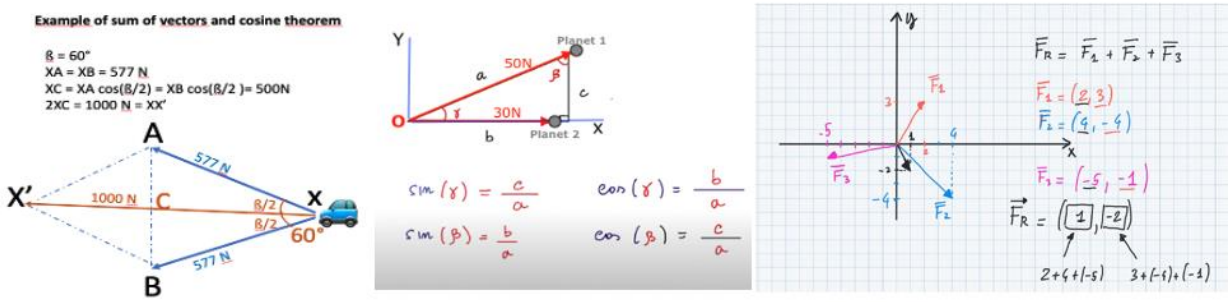

Figure 2. Vector calculation of the resultant gravitational force FR. a) Example of the sum of 2 vectors exerting equal force; b) Vector Newton forces of 2 planets and the Earth; c) Example of the sum of 3 vectors and their resultant force. We calculate the total of these vectors at any time by summing the FR (the resultant gravitational forces) of two celestial bodies, each multiplied by the cosine of the adjacent half-angle, *according to Carnot's theorem* (Figure 2,a). After placing on the abscissae the FR vector $\vec{b}$ (expressed in Newtons, henceforth "N") N(0) of Earth/Sun, with coordinates (b,0), the other vectors (n), with n ∈ (2,9), have Cartesian coordinates $\vec{a}$(n) cos γ, a(n) sin γ, with n ∈ (2,9) and constitute the N(n) force of one of the 9 planet/Earth combinations (figure 2,b). In the case of at least three forces, *the resultant gravitational force FR would be to be calculated according to the scheme in Figure 2,c.*

Consequently, the total N FR acting on the Earth at the Observation point O is: Ntot = $\sum_{n=1}^{9} MN(n)$ expressed in Newtons. Moreover, we can establish a connection between the angle γ in Figure 2,b and the angular distance value proposed in the Hypothesis 1 of this study (see *supra*, Section 2.4, Figure 1).
If we consider the sum of all abscissa values as "A," and the sum of all ordinate values as "B," the total FR N then: **FR (t) (N tot) = $^2\sqrt{(A^2+B^2)}$.**
The resulting gravitational force FR(t) (N tot) [hereinafter referred to as **FR**] provides us with the absolute magnitude or intensity of the gravitational forces exerted by the 9 planets on the observation point O, positioned on the Earth's surface at time t. *By knowing this value at any given moment, we gain insight into the changing FR acting on or around the observation point over time.*

2.9. Three index values

Three index values are used to find correlations between FR and seismic triggering for all 200 experiments.

2.9.1. Variation in FR values (σFR) within two consecutive 24-hour blocks near the earthquake.

The first index, as standard deviation (σFR) of the average FR value of *two consecutive* 24-hour (henceforth "σ***48h***FR", or parameter "A") FR blocks is calculated. From 28 to 31 values in a month (1 value every 24h, depending on the length of the month), 14-15 *cumulative index values* are derived, representing a 62-hour time slot around the earthquake. When we mention *"cumulative,"* it means that if, let's say, the index value 3 identifies the earthquake time, it implies the accumulation of time corresponding to index 1 + index 2 + index 3.
These index values are sorted such that index 1 corresponds to the highest or lowest σ***48h***FR value of the month, index 2 to the second highest or lowest, and so forth up to index 14, for a total of 28 to 31 values per month. This graph is structured with hourly FR values over a reference month, positioning the earthquake's point at *the start of the fourth week*. This approach facilitates the analysis of FR behavior in the 3 weeks preceding and 1 week following the earthquake.
These values are shown in Line 29 of the data: see Table 3 and 4.

Table 3 DOI 10.5281/zenodo.7779003, Study of FR gravitational forces exerted by the angular distances of all 9 S.S. celestial bodies toward Earth: L'Aquila Earthquake, 06.04.2009, Italy, M6.1, for Section 2.9.

For the 2009 L'Aquila (Central Italy) earthquake, the pink band around Index 5 in Figure 3 indicates the time of the earthquake. In this example, the σ***48h***FR value with Index 5 is 4.5607E-11. See the value in: Cell SG31 of the data in Table 3; Earthquake n. 85, Point 2, of the list in Table 4 (see *infra*, Section 2.10).

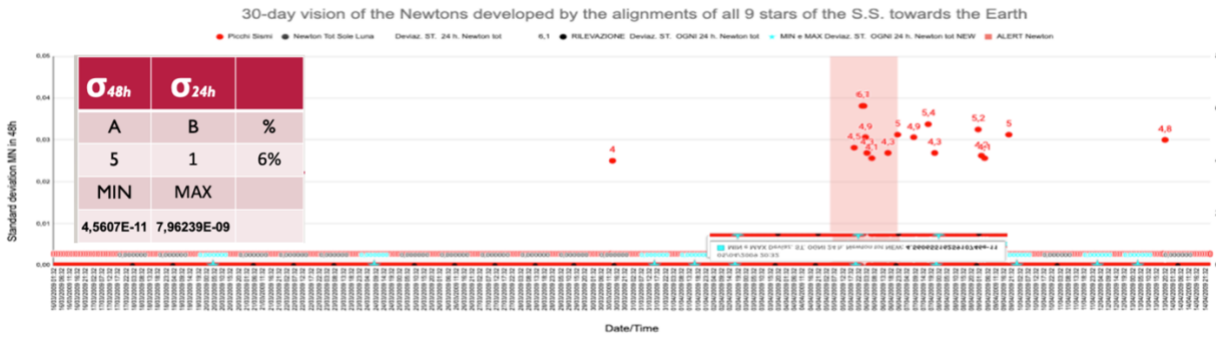

Figure 3. The cumulative percentile of Alert Time of the earthquake l'Aquila (Central Italy), 6.04.2009, M6.1. The value of parameter A (σ48hFR) with Index 5 is 4.5607E-11. The value of parameter B (σ24hFR) with Index 1 is 7,96239E-09. The percentile of the Alert Time in 1 month is 6%.

2.9.2. Variations in FR values (σFR) across 24 one-hour intervals near the earthquake

The second index, as standard deviation of the average FR values of each 24-hour (henceforth "σ***24h***FR", or parameter "B") block is calculated. A month is divided into 28/30 periods of 24 hours each, yielding 696 hourly σ***24h***FR values calculated over 24-hour periods. These values are ordered into *cumulative* (see *supra*, Section 2.9.1) 347 index values, such that index 1 corresponds to the maximum or minimum σ***24h***FR value of the month, index 2 to the second maximum or minimum, and so on up to index 347. The 696 values σ***48h***FR are in line 35 of the drive (see *supra*, Section 2.9.1, table 3 and 4).

For the 2009 L'Aquila earthquake, Index 1 corresponds to the pink band around the earthquake time in Figure 2. In this example, the value of σ***48h***FR with Index 1 is 7,96239E-09. See the value in: Cell RZ35 of the drive in Table 3, Earthquake n. 85, Point 2, of the list in Table 4 (see *infra*, Section 2.10).

2.9.3. Percentile of Alert Time affected by σFR

The third index, as a percentile of the cumulative Alert Time within one month influenced by the combined σFR indices of the parameters σ***48h***FR and σ***24h***FR for each earthquake, is calculated. It serves as a measure of the quality of the values of the first two σFRs given above. As explained, when we mention *"cumulative,"* it means that if, let's say, the index value 3 identifies an Alert Time, it implies the accumulation of time corresponding to index 1 + index 2 + index 3.

The percentile values of the Alert Time for all 200 earthquakes are listed in Table 8 (see *infra*, Section Results, 3.2.4).

The percentile of the Alert Time of 2009 L'Aquila earthquake is shown in Figure 2: in this example the Alert Time occupies the sixth percentile (6%) within a month.

2.9.4. Three lines of experimental analysis

We conducted a total of 600 gravitational force measurements around the earthquakes, with 200 measurements for each of the three following lines of analysis:

1. The gravitational forces exerted individually by the seven planets of the Solar System, the Sun, and the Moon toward Earth.
2. The gravitational force from the Luni-Solar System alone, excluding the seven planets of the Solar System directed toward Earth.
3. *The gravitational forces developed individually by the seven planets of the Solar System excluding the Sun and the Moon, toward Earth.*
Further details on the variations in data across these three Analysis Lines are discussed below (see *infra*, Section 4.2) and illustrate that the most dependable measurement, for purposes of identifying seismic triggering times and testing the hypothesis, lies within the analysis of Line 3.

2.10. Structure of the sample of 200 earthquakes

The structure of the sample of 200 earthquakes is outlined, considering a minimum magnitude of M4.3, from a total of 1,620 Italian earthquakes (ASMI-INGV Catalog) spanning from 1600 until 2022. See the earthquake list in Table 4).

Table 4 DOI 10.5281/zenodo.8171569, APPENDIX – List of earthquakes, for Section 2.9.

Among these 200 earthquakes:
- *Eighty-five were randomly selected* using the Bernoulli sampling method from the 560 earthquakes ≥M4.3 in the 1600–1899 catalog.
- *Sixty were randomly selected* using the Bernoulli sampling method from the 1,060 earthquakes ≥M4.3 in the 1900–2022 catalog.
- *Fifty-five were purposefully* chosen from the 1,060 earthquakes ≥M4.3 in the 1900–2022 catalog.

2.10.1. Reliability of the sample

The consideration of 200 earthquakes with a minimum magnitude of M4.3, out of a total of 1,060 earthquakes in Italy from 1900 until 2022, constitutes a sample size of about 19% of the total. The sample selection includes the following.
1. One hundred and forty-five were chosen through Bernoulli sampling, representing 72.5% of the total, using a simple random sampling method. Each of these 145 units in the earthquake population had an equal probability of being included in the sample.
2. Fifty-five additional earthquakes were discretely chosen for study interest due to their occurrence within the last 120 years, making them earthquakes ≥M4.3.
A short video (see Table 6) demonstrates an example of the random sample extraction method used for selecting the 145 earthquakes.

Table 5 DOI 10.5281/zenodo.8083305, Random sample extraction of 145 earthquakes, for Section 2.10.1.

Note: During random sampling, earthquakes were substituted under certain conditions:
1. For foreign earthquakes (e.g., Slovenia), the model does not consider earthquakes outside Italy.
2. For earthquakes at sea (e.g., Tyrrhenian Sea), the model does not consider seaquakes.
3. For aftershocks occurring within one Moon phase of a mainshock, the parameters of Hypothesis 2 did not accurately detect the earthquake, possibly due to astronomical parameters not significantly influencing subsequent earthquakes following a strong mainshock.
4. Earthquakes were also replaced due to repetitions of already drawn numbers.

3. Results

3.1. Hypothesis 1

Analyzing 200 Italian earthquakes spanning from 1600 until 2022, a correlation between planetary positions and earthquake magnitudes emerged.

3.1.1. A Statistical correlation between planetary positions and earthquake magnitudes

Hypothesis 1 is substantiated: a statistical correlation exists between the positions of the planets, the Moon, and the Sun and earthquake magnitude. A recurring correlation between *angular measurements* of conjunctions and oppositions of the 36 pairwise combinations of the seven planets of the Solar System, the Moon, and the Sun and the magnitude intervals (Richter) of 200 Italian earthquakes ≥M4.3 (using ASMI-INGV data spanning from 1600 until 2022) is evident for both the 200 earthquakes since 1600 and the 63 earthquakes that occurred after 1988, which are also part of the 200-earthquake dataset analyzed. *This serves to assess the reliability of the earthquake catalog utilized for this study,* as will be discussed later (see *infra*, Section 4.6).

A trend toward higher average earthquake magnitudes corresponds to *more numerous and accurate alignments* of planet pairs: *more alignments are directly related to higher earthquake magnitudes.*
There is an *inverse correlation* between the magnitude of earthquakes *and the average angular distance* of planets from Earth and a *direct correlation* between the magnitude of earthquakes and the *number of planets in line* with Earth.
Besides, *the Moon's angular position does not substantially alter earthquake magnitude trends.* Although slight differences emerge when considering alignments of 36 planet pairs with the Sun and Moon or when excluding the Moon considering only 28 alignments, the trends remain consistent. (see Figure 4 and 5).

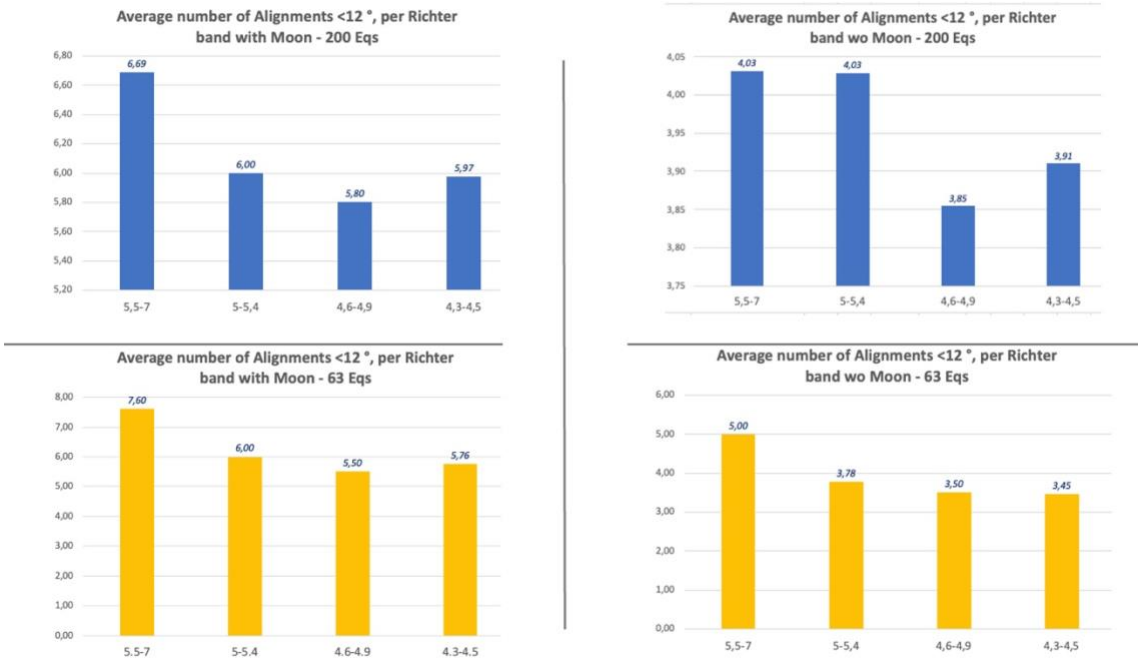

Figure 4. Distribution of average number of alignments <12° by magnitude range of earthquakes occurring after 1988. Average number of alignments <12° for each magnitude range (Richter), with the Moon (left graph) and without (right graph) at the triggering time of both the 200 earthquakes since 1600 and the 63 earthquakes that occurred after 1988. *The average number of alignments rises as the magnitude increases.*

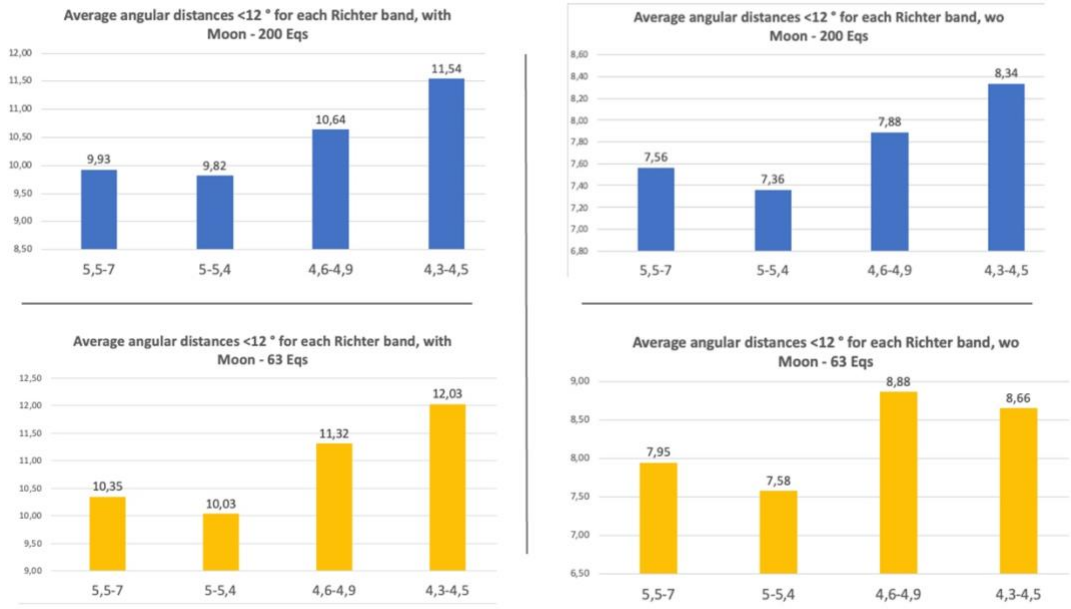

Figure 5. Distribution of average angular distance <12° by magnitude range of the 200 earthquakes. Average angular distance <12° for each magnitude range (Richter), with the Moon (left) and without (right graph) at the triggering time of both the 200 earthquakes since 1600 and the 63 earthquakes that occurred after 1988. *The average angular distance of alignments decreases as the magnitude increases.*

The observation that an increase in the magnitude of earthquakes corresponds to both an increase in the number of pairs of planets with close angular distance and a decrease in angular distance from Earth is *in line with Newton's Law of Universal Gravitation* (Newton 1687).

3.1.2. The distribution of the 200 average angular distances is normal

The distributions of average angular distance values (of Solar System bodies relative to the Observer on Earth) at the time of seismic triggering, for both the sample of 200 earthquakes since 1600 and the 63 earthquakes that occurred after 1988, *are normal.* The normality of the distributions was validated with a 95% confidence interval using the Shapiro-Wilks and *P-value tests (see Figure 6), with a p-value >0,05.* Thus, this is a *normal distribution* of the data suggesting that the distribution of these values *is not random.*

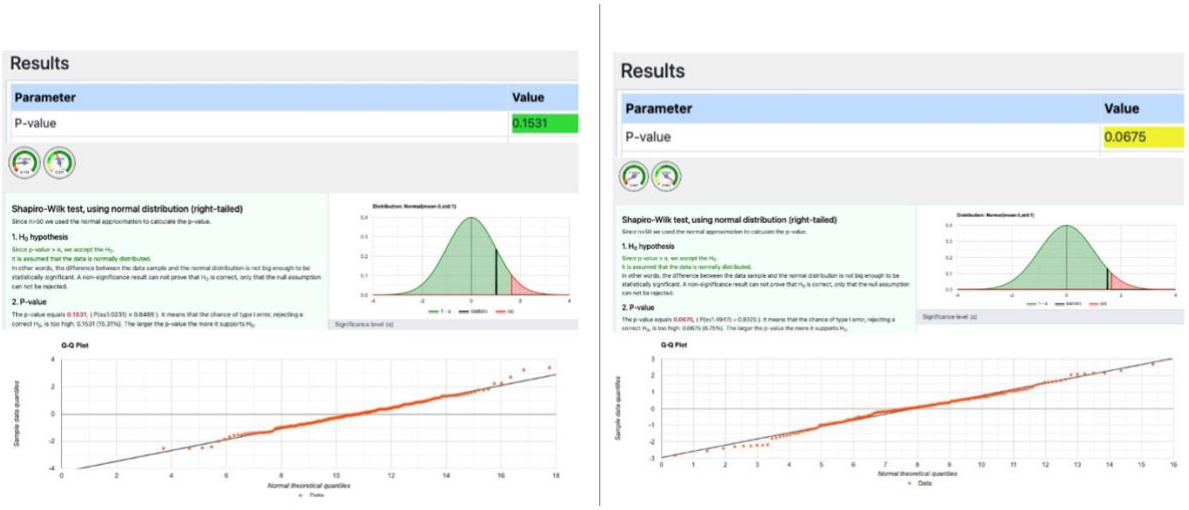

Figure 6. Normal distribution of average angular distances <12° at the trigger time of the 200 earthquakes. The distribution of the 200 average angular distances <12° at the time of seismic

triggering (with the Sun and the Moon on the left, without the Moon on the right) is validated with a 95% confidence interval using the *Shapiro-Wilks and P-value tests*, *with a p-value of 0.1531 (left graph).* Interestingly, the average angular distances calculated including the Moon along with the seven planets and the Sun showed a better fit to a normal distribution compared to the same calculations excluding the Moon, that shows *a p-value of 0,0675 (right graph)*. The p-value for the distribution of average angular values including the Sun and Moon of the sample of 63 earthquakes that occurred after 1988 is 0.0506. While the p-value excluding the Moon from the calculation is 0.1542 (see Table 6). *The normality of all distributions in this section was then validated with a p-value >0.05.*

Table 6 presents the Excel file containing analytical and comparative outcomes between the two calculations: with the Sun and Moon and without the Moon, for both the sample of 200 earthquakes since 1600 and the 63 earthquakes that occurred after 1988.

Table 6 DOI 10.5281/zenodo.10058522, Summary Excel tables of results of the first hypothesis, for both the sample of 200 earthquakes since 1600 and the 63 earthquakes that occurred after 1988, for Section 3.1.

3.2. Hypothesis 2

In Sections 3.2.1 to 3.2.4 we will show the results of FR indices (see *supra*, Section 2.9). Whereas in Section 3.2.5 we will show the results of FR values, from which the indices originate.
Overview and details of the 200 analyzed earthquakes, including the values and indices for the σFR parameters A, B and the percentile of the alert time in the three lines of analysis, are provided in Table 9 and 10 (see *infra*, Section 3.2.6).

3.2.1. The σFR indices distributions

The initial outcome deduced from assessing the Hypothesis 2 is the presence of two non-random distributions in the range of the three σFR indices (parameters A, B and % Alert Time) of the 200 earthquakes.
Results were well approximated using logarithmic functions Y = ln(x) for σFR values and *polynomial functions* of the form $a+bx+cx^2+dx^3+\ldots dx^n$, where $n \in (1.8)$ for σFR indices and for the percentile of the Alert Time.
The regression R^2 values (as shown in the example in Figure 7) *result close to 1*, indicating *a strong fit between theoretical and real distributions* of the three σFR indices (parameters A, B and % Alert Time) for all the 200 earthquakes.

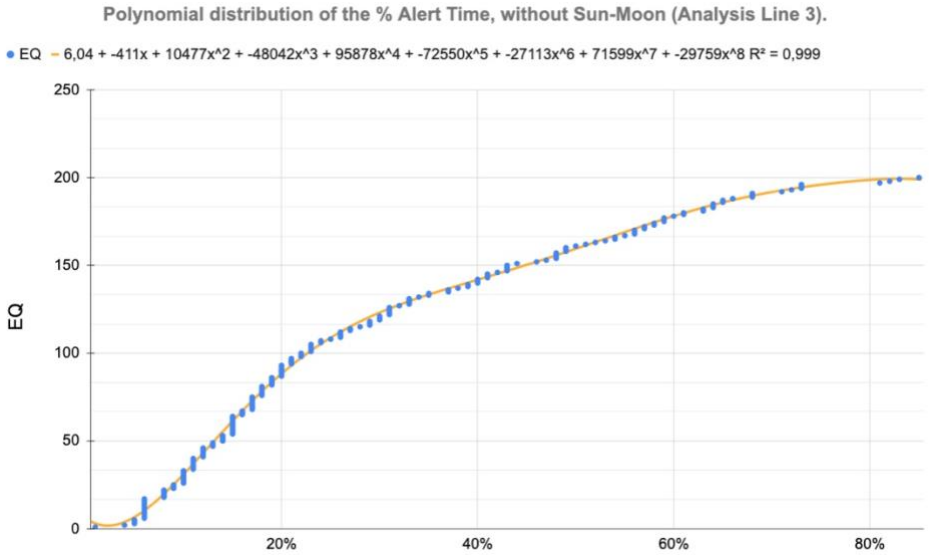

Figure 7. Polynomial distribution of the % Alert Time, without Sun-Moon (Analysis Line 3). Notably, the most reliable distribution for identifying seismic trigger Alert Times for all 200 earthquakes is *the formula describing the distribution of percentile Alert Time* influenced by σFR during triggering within 1 month, *found in Analysis Line 3*: $\boldsymbol{Y = 6.04-411x+10477x^2-48042x^3+95878x^4-72550x^5-27113x^6+71599x^7-29759x^8}$ (See Table 8 for details). This particular polynomial distribution boasts an *impressive regression coefficient R^2 of 0.999, the closest value to 1 in the entire study.* This result holds true when compared to the R^2 values of the other two Analysis Lines (see *infra*, Figure 8).

It follows that new data regarding a 201st earthquake (σFR indices, values and percentiles of the Alert Time of an nth earthquake) could likely be placed on the distribution curve with minimal error. Excluding the Sun and Moon from the angle calculations resulted in R^2 being closer to a value of 1 than the calculation including them. So, *Analysis Line n.3 was identified as the most promising due to its regression index R^2 closest to 1* ("all planets, without Moon and Sun", see *supra,* Section 2.9.4). The summarized regression R^2 coefficients are presented in Figure 8.

Regression index R^2	All Planets	Moon and Sun	All Planets without Moon and Sun	Theoretical Distribution
R^2 Index values σ48hFR (param. A)	0,969	0,971	**0,979***	*Polynomial*
R^2 Values σ48h FR (param. A)	0,905	0,885	**0,959***	*Logarithmic*
R^2 Index values σ24hFR (param. B)	0,99	0,991	**0,996***	*Polynomial*
R^2 Values σ24hFR (param. B)	0,864	0,896	**0,982***	*Logarithmic*
R^2 % of Alert Time in a month	0,998	0,998	**0,999***	*Polynomial*
* = Best Rate				

Gravitational forces of seismic triggering of 200 Earthquakes: comparative table of regression coefficients of empirical vs. theoretical distribution.

Regression index R^2	All Planets	Moon and Sun	All Planets without Moon and Sun	Theoretical Distribution
R^2 Index values σ48hFR (param. A)	0,961	**0,98***	0,959	*Polynomial*
R^2 Values σ48h FR (param. A)	0,91	0,843	**0,958***	*Logarithmic*
R^2 Index values σ24hFR (param. B)	0,985	0,99	**0,995***	*Polynomial*
R^2 Values σ24hFR (param. B)	0,842	0,895	**0,961***	*Logarithmic*
R^2 % of Alert Time in a month	0,996	**0,998***	0,996	*Polynomial*
* = Best Rate				

Gravitational forces of seismic triggering of 63 Earthquakes (since 1988): comparative table of regression coefficients of empirical vs. theoretical distribution.

Figure 8. Summary/comparative table of the R^2 regression coefficients of the 3 parameters identifying σFR. This table presents a summary and comparison of the regression R^2 coefficients for the three σFR indices (parameters A, B, and % Alert Time) for both the 200 earthquakes (on the left) and the 63 earthquakes occurring after 1988 (on the right) across the three lines of analysis. Notably, the regression coefficient R^2 of 0.999 in Analysis Line No. 3 (on the left) is the closest value to 1 in the entire case study. Similarly, the right graph, representing the R^2 regression coefficients for the 63 earthquakes occurring after 1988, yields results very similar to those on the left, indicating once again that *Analysis Line No. 3 exhibits values closest to 1*, than the other two, even for the most recent sample of earthquakes.

The comprehensive examination of the R^2 regression coefficients of the 200 earthquakes being studied, including Parameters A and B, as well as the percentiles of Alert Time within a one-month period across the three Analysis Lines, is illustrated in Table 7.

Additionally, Table 7 presents identical analysis for the *63 earthquakes occurring after 1988,* which are also part of the 200-earthquake dataset analyzed. *This serves to assess the reliability of the earthquake catalog utilized for this study,* as will be discussed later (see *infra*, Section 4.6).

Table 7 DOI 10.5281/zenodo.10058668, **Summary graphs of the data distributions of the** Hypothesis 2**, with the R^2 regression values** of the three σFR values and indices (parameters A, B and % Alert Time) of both the 200 earthquakes and the 63 earthquakes after 1988, for Section 3.2.

3.2.2. The σFR concentration of data at lower values

A second result comes from the analysis of the *σFR indices obtained: they are concentrated around very low values.*

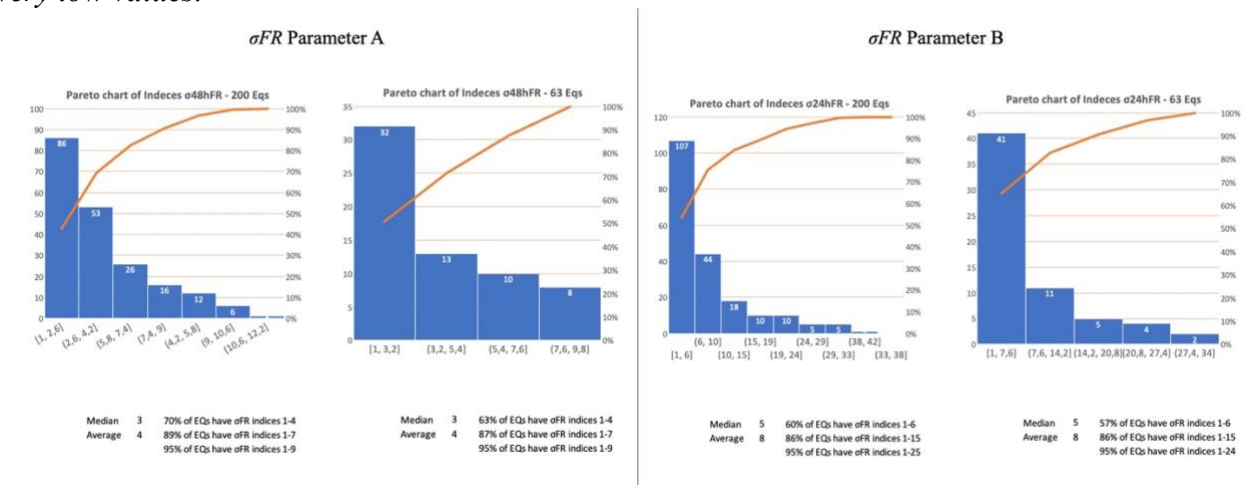

Figure 9. **Distribution of σFR indices of parameter A (left graph) and of parameter B (right graph).** This figure presents a summary of the distribution and a comparison of σFR indices between the sample of 200 earthquakes and the sample of 63 earthquakes within the reference month for both parameter A (Left) and parameter B (Right). Following the line of analysis No. 2 graphs show that both distributions have a *median value (parameter A) of 3* and 95% of the earthquakes are concentrated within a low σFR index value of 9 (the maximum possible σFR index value is 14, see *supra*, Section 2.9.1); For the other σFR index (parameter B), however, both distributions have *a median value of 5*, and 95% of the earthquakes are concentrated within a consistently low σFR index value of 24-25 (the maximum possible σFR index value is 347, see *supra*, Section 2.9.2). As explained, index 1 corresponds to the highest or lowest σFR value of the month, index 2 to the second highest or lowest value, and so on. For the remaining lines of analysis, specifically No. 1 and 3, *the data concentration shows a striking similarity for both the 200 earthquakes since 1600 and the 63 earthquakes that occurred after 1988*. Refer to Table 8 for details.

The concentration of σFR indices at such low values for both parameters A and B gives us a useful indication: *earthquakes are triggered by high or low σFR values, while moderate σFR values do not trigger earthquakes* (See *supra*, Graphical Abstract).
Table 8 summarizes the values of the three σFR indices (parameters A, B, and % Alert Time) for:
- both the 200 earthquakes from 1600 to 2022 and the sample of 63 earthquakes after 1988;
- for the three lines of Analysis (see *supra*, Section 2.9.4).

Additionally, Table 8 presents identical analysis for the 63 earthquakes occurring after 1988, which are also part of the 200-earthquake dataset analyzed. *This serves to assess the reliability of the earthquake catalog utilized for this study,* as will be discussed later (see *infra*, Section 4.6).

Table 8 DOI 10.5281/zenodo.10058786, **Summary distribution and probability** of the three σFR indices (parameters A, B and % Alert Time) **of the** Hypothesis 2 for both the 200 earthquakes and the sample of 63 earthquakes after 1988, for the three lines of Analysis.

Overview and details of the 200 analyzed earthquakes, including the indices for the σFR parameters A and B are provided in Table 9 and 10 (see *infra*, Section 3.2.6).

3.2.3. The probability distribution of σFR

A third outcome results from the probability analysis by which we obtained the values of the three σFR indices (parameters A, B and % Alert Time) of the 200 earthquakes.

The statistical probability that the three observed σFR indices (parameters A, B, and % Alert Time) had those low values for the three lines of analysis is also significantly reduced for the 200 earthquakes, with a probability of less than $3.18x10^{-34}$. While for the 63 earthquakes the probability is less than $2.81x10^{-11}$.

The calculation of the statistical probability of the three σFR indices (parameters A, B and % Alert Time) of both the 200 earthquakes and the sample of 63 earthquakes after 1988, at the time of seismic triggering for the three lines of analysis, is presented in Table 8.

3.2.4. The distribution of percentile Alert Time

In Table 8 (see *supra*, Section 3.2.2) we examined the histogram and Pareto plot of the σFR indices and percentiles *of the Alert Times* affected within one month of both the sample of 200 earthquakes and the sample of 63 earthquakes after 1988. All three lines of analysis of both samples show a *clear concentration of results in a narrow range of values.*

By correctly applying the two parameters of σFR A and B, it is possible, for example, for Analysis Line 1 to observe that not less than 64 percent of both the 200 earthquakes and the 63 earthquakes occurring after 1988 fall within just 25 percent of the Alert Time for the reference month (see Figure 10).

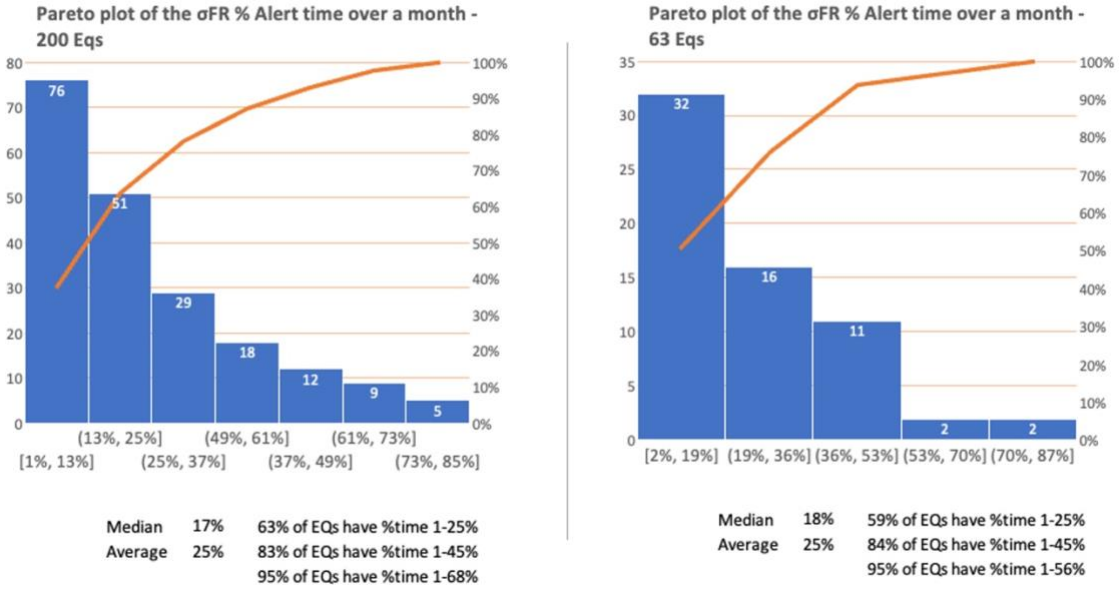

Figure 10. Pareto plot of the percentile Alert time over a month. This figure presents a summary and comparison of the σFR % Alert Time for both the 200 earthquakes (on the left) and the 63 earthquakes occurring after 1988 (on the right) for the reference month. Following the line of analysis No. 1 graphs show that both distributions have a median % Alert Time value of 17-18%. Besides, *95% of the earthquakes are concentrated within a narrow % Alert Time of 56-68%.* For the remaining lines of analysis, specifically No. 2 and 3, *the data distribution (Pareto plots and histograms) also shows a striking similarity* for both the 200 earthquakes since 1600 and the 63 earthquakes that occurred after 1988: refer to Table 8 for details.

By integrating the findings from the Pareto chart with the previously discussed R^2 regression indices (see *supra*, Section 3.2.1), it becomes highly probable that a newly assigned percentile Alert Time

value (X) for a specific n^{th} earthquake (Y), influenced by the same σFR during seismic triggering, *can be situated on the same theoretical curve with minimal error*.
The concentration of 95 percent of earthquakes in a reduced % Alert Time frame in all three Analysis Lines, indicating measurable and *probably non-random behavior,* allows these data to be used to contribute to a *plausible earthquake prediction model*.
Overview and details of the 200 analyzed earthquakes, including the % Alert Time in the three lines of analysis, are provided in Table 9 and 10 (see *infra*, Section 3.2.6).

3.2.5. The range of σFR values for seismic triggering

Now let's talk about σFR values. The summarized σFR values are presented in Table 8 (see *supra*, Section 3.2.2).
Based on the 200 experiments, it is also possible to establish the range of σFR values for both Parameters A and B that can confidently indicate *that earthquakes ≥M4.3 will not occur beyond these values.* This confidence arises because the values align along a theoretical logarithmic-type curve with a regression index R^2 very close to 1.
For example, Table 8 (see *supra*, Section 3.2.2) shows for Analysis Line 3 the identification σFR Parameter A values ranging from a minimum of 2.32×10^{-28} (6.29×10^{-26} for the 63 earthquakes since 1988) to a maximum of 4.90×10^{-16} (8.56×10^{-17}), and σFR Parameter B values ranging from a minimum of 3.36×10^{-32} (7.00×10^{-30}) to a maximum of 5.88×10^{-18} (8.20×10^{-17}) within the values of the theoretical polynomial curve mentioned earlier (see *supra*, Section 3.2.1).
The orders of magnitude of the maximum and minimum values of σFR *appear congruent,* for both the 200 earthquakes since 1600 and for the 63 earthquakes that occurred after 1988.
Overview and details of the 200 analyzed earthquakes encompassing values for σFR Parameters A and B are provided in Table 9 and 10 (see *infra*, Section 3.2.6).

3.2.6. Overview and details of the 200 analyzed earthquakes

Overview of the 200 earthquakes analyzed including the values and indices for the parameters σFR A, B and the percentile of the Alert Time in the three Lines of Analysis is given in Table 9.

Table 9 DOI 10.5281/zenodo.10061252, **Overview of the 200 analyzed earthquakes encompassing values and indices for σFR Parameters A, B, and the percentile of Alert Time across the three Analysis Lines.**

Details of the 200 earthquakes analyzed including the values and indices for the parameters σFR A, B and the percentile of the alert time in the three lines of analysis are given in Table 10. This table encompasses the 200 Excel calculation files, with 3 tabs for each, because of the three Analysis Lines.
In each of the 600 Excel sheet tabs (200 tabs for each of the 3 Lines of Analysis) the main values are:

- Index σFR Parameters A: cell A36
- Index σFR Parameters B: cell A26
- Value σFR Parameters A: cell A25
- σFR Parameters B value: cell A23, if minimum value
- σFR Parameters B value: cell A24, if maximum value
- Percentile of alert time in the month: cell A34

Table 10 DOI 10.5281/zenodo.8163189, **Overview and details of the 200 analyzed earthquakes encompassing values and indices for σFR Parameters A, B, and the percentile of Alert Time across the three Analysis Lines.**

The earthquakes list in Table 4 is also relevant here (see *supra*, Section 2.10).

4. Discussion

In this chapter, the author of this paper highlights key aspects for discussing the two hypotheses put forth in this study: whether the gravitational influences of the seven planets of the Solar System, along with the Moon and the Sun, can truly impact earthquake triggering (Hypothesis 2) and their magnitudes (Hypothesis 1).
Additionally, considerations are made regarding the different values of FR and tidal force exerted by celestial bodies in the Solar System on Earth.
I also address a portion of the literature that failed to find a causal relationship between tides and seismic triggering, using the results of this study to demonstrate that these theories do not contradict our findings.

4.1. Comparison with previous studies

The results of this study are not congruent with previous studies that have addressed correlations between earthquakes and planetary positions. Chinese and Indian schools, as well as smaller Italian investigations, have mainly focused on demonstrating the co-occurrence of conjunctions or oppositions of celestial bodies for specific earthquakes and have not provided in-depth statistical results (see *supra*, Section 1.3).

4.3. Gravitational and tidal forces in the Solar System

Considering the tidal accelerations exerted by planets on Earth, tides stem from the difference between gravitational acceleration within Earth and at its center. Moon and sun is causative agent in the formation of tides. Tidal is a natural phenomenon caused by the gravitational force of attraction between moon and sun [31]. Tidal forces decrease inversely with the cube of distance. Notably, gravitational forces diminish inversely with the square of the distance between objects.
The following table highlights the comparative orders of magnitude for maximum tidal forces from the seven planets versus the Moon's impact on Earth (Figure 10). Intriguingly, the *Sun's gravitational attraction FR on Earth exceeds the Moon's by over 166 times at perigee and perihelion, while the Sun's tidal force is only 41% of that of the Moon's.*

Comparison table of the gravitational and tidal force exerted on Earth by Solar System celestial bodies at the perigee

	Mass (10^24kg)	Perigee 10^9 (billions of m.)*	Max gravitational acceleration per mass unit	Max gravitational acceleration (% of Moon)	Max Tidal Force per mass unit	Max Tidal Force (% of Moon)
SUN	1.989.000,000	147,00	6,14E-03	16614,6235%	5,33E-07	41,03%
MERCURY	0,330	82,50	3,23E-09	0,0088%	5,00E-13	0,00003851%
VENUS	4,870	39,79	2,05E-07	0,5552%	6,58E-11	0,00506529%
MOON	0,073	0,36	3,70E-05	100%	1,30E-06	100%
MARS	0,642	55,65	1,38E-08	0,0374%	3,17E-12	0,00024408%
JUPITER	1.898,000	591,97	3,61E-07	0,9777%	7,78E-12	0,00059951%
SATURN	568,000	1.204,28	2,61E-08	0,0707%	2,77E-13	0,00002131%
URANUS	86,800	2.586,88	8,65E-10	0,0023%	4,27E-15	0,00000033%
NEPTUNE	102,000	4.311,02	3,66E-10	0,0010%	1,08E-15	0,00000008%

* Credit : J.E. Arlot, IMCCE/observatoire de Paris

$$Gravitational\ Accelaration\ a=\frac{GM}{r^2}$$

$$Tide\ force \quad T=-\frac{da}{dr}R=\frac{2GM}{r^3}R$$

$$R:\ radius\ of\ the\ Earth$$

Figure 11. Chart of the gravitational and tidal force per mass Earth unit at the perigee. This is a comparative table of the tidal and gravitational forces exerted by celestial bodies in the Solar System

at perigee. These insights emphasize the significant differences in gravitational and tidal components between celestial bodies in the Solar System.

4.4. Gravitational force as a component of vertical tidal force

The answer to this question lies in the experimental findings of this study, specifically in the behavior of the resulting gravitational forces (σFR) from the Sun, Moon, and the seven planets of the Solar System. Given that earthquakes occur when the fault reaches a critical energy threshold and the vertical tide's component can contribute to the trigger (see *supra*, Section 2) it is suggested that *σFR is a contributor to the vertical tidal force that influences seismic activity.*

This hypothesis emerges considering the experimental trends and behaviors, although it *does not establish a direct cause-and-effect mechanism between gravitational forces and vertical tides*. Yet, the observed bidirectional relationship between the positions of celestial bodies, gravitational forces, and earthquakes *supports the idea that the σFR play a role in the vertical tidal force.*

4.5. Gravitational force and gravity acceleration

The gravitational force between masses m and M is described by Newton's law of gravity (with G as the gravitational constant): $Fg = GmM / r^2$, where r is the distance. Gravitational acceleration (force per unit mass) of body M due to body m can be defined as $a = Fg / m = GM / r^2$, as per Newton's second law.

In this study, we could have used acceleration of gravity, but since Earth's mass is constant and the focus is on the change in force (σFR) during earthquakes, not the force magnitude (see *supra,* Section 2.12), Earth's mass does not affect the outcome. *Whether Earth's mass is included or excluded, the index values of σFR remain the same.*

The gravitational force (FR) is a component of the tidal force. Tides stem from the difference in gravitational attraction between different parts of a celestial body. Newton's law of gravity ($Fg = GmM / r^2$) describes the force between masses m and M. The variation of attraction between two objects located at distances r and r+dr is obtained by deriving the expression of gravitation relative to r: $dF / dr = -GMm/r^3$, revealing the *tidal effect to be inversely proportional to the cube of distance.* For the Earth–Sun system, the tidal force is about half that of the Earth–Moon system due to the $r^3 =$ r x r^2 relationship.

While tidal force could be used in calculations, it does not change the outcome of σFR, similar to gravity. Adding or removing *1/r* in calculations would yield *identical σFR index values.*

4.6. The reliability of the ASMI-INGV catalogs

The scientific significance of the manuscript can be also questioned. For this study, the quality of the seismicity catalog is essential. It can be argued that the catalog is complete (covers all earthquakes above the magnitude threshold) for the entire period analyzed (1600-2023). The accuracy of the time of occurrence of historical earthquakes can be questioned. Therefore, this point needs careful verification.

Regarding the catalog's quality, it's essential to understand that conducting a scientific study relies on using the data from this source. It's worth noting that this is the sole official catalog in Italy, managed by INGV, and represents the most authoritative data source available. The Italian Historical Macroseismic Archive ASMI [28] offers access to information on over 6500 Italian earthquakes spanning from 461 BC to 2020, extracted from more than 430 seismological investigations.

For each earthquake, various studies based on the ASMI catalog are accessible*, and the results, concerning dates and times for each earthquake*, are the most plausible among the multiple hypotheses presented in the referenced studies.

We compared the results of Hypothesis 1 and Hypothesis 2 by considering *63 earthquakes* out of the 200 M≥4.3 in the entire list, all of which *occurred after 1988*. These earthquakes are more recent and thus were subject to further analysis.

For these 63 earthquakes we then considered the *National Seismic Network (RSN), Italy's permanent nationwide seismological network*, managed by the National Institute of Geophysics and Volcanology (INGV) with contributions from collaborating institutions and observatories [32]. Metadata have been *available online since 1988*, thus constituting an accurate time reference for each earthquake that has occurred.
In this study, we consistently compared the outcomes of the analysis involving all 200 earthquakes with those derived from the examination of the 63 most recent earthquakes M≥4.3. The findings related to Hypothesis 1 and Hypothesis 2 for the smaller and more recent sample of 63 earthquakes *were consistent with those obtained from the larger and less recent sample of 200 earthquakes.*

5. Conclusion

This study's main conclusion is that seismic triggering for earthquakes M≥4.3 is driven not by the absolute gravitational force from celestial bodies but *by extreme stability or instability of the standard deviation of FR (σFR) within a 24–48-hour window*.
The quantification of the tidal force range and resulting gravitational force (FR) values for seismic triggering had not been previously attempted, *nor had an approximate theoretical formula for identifying the stress point of a fault* and the need for energy release been formulated. In terms of the first calculation, this study computed the σFR resulting from celestial bodies in the Solar System on Earth.
A recurring range of σFR values (standard deviation of FR) was established around seismic trigger on the Earth: outside this σFR range, the occurrence of earthquakes ≥M4.3 was *highly unlikely.*
The cumulative gravitational/tidal force from these bodies acting on a specific Earth point determines the stability parameter for vertical tidal force and seismic triggering.
This approach of calculating the resultant gravitational force in terms of change value (σFR) instead of absolute value (FR) *marks a substantial departure from existing literature.* Additionally, earthquake magnitudes seem to correlate with planetary conjunctions/oppositions, with the Moon possibly playing a less significant role than commonly assumed.

5.1. Indirect data measurement

This study does not employ direct ground-based measurements via gravimeters for understanding Earth's seismic triggers due to external gravitational forces. Instead, it innovatively utilizes *computational methods relying on ephemerides (planet positions),* azimuth-elevation coordinates, and vector physics. This indirect method calculates FR for each instant at earthquake locations.

5.2. Broader influence of planets

Contrary to conventional beliefs, *the most reliable σFR* distribution for seismic triggers across 200 experiments omits the Moon and Sun from the computation (see *supra,* Figure 8 in Section 3.2.1). While their gravitational and tidal forces are less than those exerted by the Sun and Moon, the gravitational forces generated by the seven planets within the Solar System exhibit a meaningful correlation with Earth's tidal influences. In essence, *the somewhat modest impact of these planetary gravitational forces introduces a disruptive factor that fosters seismic triggers.*

5.3. Vertical tidal component on fault

FR values from the Sun, the Moon, and the seven planets create a vertical tidal component toward Earth's crust, where earthquake-triggering faults are situated. This influence extends beyond a single fault, affecting a larger region of Earth, roughly matching the locations of the examined earthquakes. Earthquakes materialize when the fault reaches a critical threshold, wherein the vertical tide's component influences triggering. This can occur in diverse ways based on tectonic context—lithostatic loading encourages normal faults while hindering reverse faults (see *supra*, Section 2).

5.4. Applying study results for earthquake forecasting

These preliminary study findings suggest considering an exponential distribution model involving two components, A and B, of the standard deviation of FR (σFR) from the Solar System's seven planets, the Sun, and the Moon during earthquakes. *This model could potentially help reduce uncertainty in earthquake timing predictions.* Using these results, up to 35% of the time an earthquake warning is given in a person's lifetime can be eliminated for the 95th percentile of earthquakes ≥M4.3. This implies that 95% of earthquakes fall within a maximum of 65% of the potential earthquake warning time of a month, with a median of 17%, a pattern worth exploring for its possible *non-random nature.*

5.5. Frequency of astronomical phenomena

The analyzed period covers 422 years, during which Earth aligns with at least one planetary pair numerous times—roughly every 193 days for each planet. Calculations based on average synodic times for planet–Sun–Earth conjunctions/oppositions reveal that *Earth aligns with the Sun and another planet every approximately (193/8 planets) 24 days.*

Over these 422 years, around 1,590 earthquakes ≥M4.3 have occurred, translating to an average of about one every 97 days.

Utilizing VS0P87 processing, an average of at least one alignment ≤12° angular distance occurs every 1.5 days between the seven planets, the Sun, and the Moon relative to the Earth. This implies that the 422-year period experiences a *substantial frequency of angular alignments from the oppositions and conjunctions described in Hypothesis 1, and these alignments are not negligible.*

5.6. Importance of a comprehensive approach

While the current model demonstrates a non-random correlation between planetary angular positions and earthquakes, it lacks the precision necessary for "good predictions" in terms of time and space. *Combining this correlation model with a multidisciplinary approach and suitable ground-based instrumentation might yield more accurate forecasts*. Detecting seismic precursors (see also *supra*, Section 1.2) such as small earthquakes [8], magnetic phenomena [5], neutron emissions [4], radio waves [3], and radon [9] could aid in definitively identifying the epicentral zone. While future ephemerides and modeling could provide time "windows," ground-based instrumentation is essential for precise epicenter and magnitude determination.

Presently, seismographic prediction models, such as those utilizing ground-based instrumentation, can accurately predict earthquake magnitudes. However, establishing a widespread and dependable ground-based *instrumental network, especially in Italy, remains a significant financial challenge in the near term.*

5.7. Study limitations for effective earthquake forecasting

Given the nearly daily frequency of these alignments, it is challenging to establish a strong correlation between them and earthquake magnitudes, and it requires complex statistical verification—a subject for future studies. Consequently, *predictions based solely on the presented astronomical model are likely to yield numerous false alerts, rendering them impractical for effective earthquake forecasting.*

In the case of the 2009 L'Aquila (Central Italy) earthquake (see, *supra*, Section 2.9.3), we saw that the percentage of Alert Time found by analyzing the lowest FR indices was 6%. A very good percentage, which allowed in that case to eliminate 94 percent of the time in a month, identifying a very narrow time in which *theoretically the Civil Defense Authorities could have concentrated.*

The crucial point to note is that 95% of earthquakes with a magnitude of ≥M4.3 don't exhibit such a low percentile of Alert Time but instead occur within 65% of the Alert Time within one month, as shown above (see *supra*, Section 3.2.4). This finding while an important result of our study, *if used alone, however proves to be a significant practical obstacle to a "good seismic forecasting" at least for earthquakes ≥M4.3.*

References

[1] H. Yanben, L. Zhian, and H. Hui, "Interdisciplinary Studies of Astronomical Factors and Earthquakes in China," in *Geodesy on the Move*, vol. 119, R. Forsberg, M. Feissel, and R. Dietrich, Eds., in International Association of Geodesy Symposia, vol. 119. , Berlin, Heidelberg: Springer Berlin Heidelberg, 1998, pp. 465–471. doi: 10.1007/978-3-642-72245-5_77.

[2] M. Kachakhidze, N. Kachakhidze-Murphy, B. Khvitia, and G. Ramishvili, "Large Earthquake Prediction Methods," *OJER*, vol. 08, no. 04, pp. 239–254, 2019, doi: 10.4236/ojer.2019.84014.

[3] V. Straser, D. Cataldi, G. Cataldi, and G. G. Giuliani, "Pre-Seismic Signals Recorded By The Italian RDF Network Before The Occurrence Of Some Earthquakes In Northern Italy," *International Journal of Software & Hardware Research in Engineering*, vol. 9, no. 1, Jan. 2021, doi: 10.26821/IJSHRE.9.1.2021.9123.

[4] A. Carpinteri and O. Borla, "Acoustic, electromagnetic, and neutron emissions as seismic precursors: The lunar periodicity of low-magnitude seismic swarms," *Engineering Fracture Mechanics*, vol. 210, pp. 29–41, Apr. 2019, doi: 10.1016/j.engfracmech.2018.04.021.

[5] Rod. Wolf, "On the periodic return of the minimum of sun-sport; the agreement between those periods and the variations of magnetic declination," *The London, Edinburgh, and Dublin Philosophical Magazine and Journal of Science*, vol. 5, no. 29, pp. 67–67, Jan. 1853, doi: 10.1080/14786445308646906.

[6] J. F. Simpson, "Solar activity as a triggering mechanism for earthquakes," *Earth and Planetary Science Letters*, vol. 3, pp. 417–425, Jan. 1967, doi: 10.1016/0012-821X(67)90071-4.

[7] V. Marchitelli, P. Harabaglia, C. Troise, and G. De Natale, "On the correlation between solar activity and large earthquakes worldwide," *Sci Rep*, vol. 10, no. 1, p. 11495, Jul. 2020, doi: 10.1038/s41598-020-67860-3.

[8] G. Riga and P. Balocchi, "Information and Predictive Oscillators of Energy Earthquakes," *OJER*, vol. 08, no. 03, pp. 201–222, 2019, doi: 10.4236/ojer.2019.83012.

[9] C.-C. Fu *et al.*, "Gamma Ray and Radon Anomalies in Northern Taiwan as a Possible Preearthquake Indicator around the Plate Boundary," *Geofluids*, vol. 2019, pp. 1–14, Sep. 2019, doi: 10.1155/2019/4734513.

[10] F. Di Stefano *et al.*, "Natural radioactivity and radiological hazard for humans: A simple introduction for newbies and students. New perspectives and innovative teaching methods," *Atti Accad. Pelorit. Pericol. Cl. Sci. Fis. Mat. Nat.*, vol. 99, no. S1, pp. A40-1-A40-12, Sep. 2021, doi: 10.1478/AAPP.99S1A40.

[11] V. Gitis, A. Derendyaev, and K. Petrov, "Analyzing the Performance of GPS Data for Earthquake Prediction," *Remote Sensing*, vol. 13, no. 9, p. 1842, May 2021, doi: 10.3390/rs13091842.

[12] Ö. Aydan, *Earthquake Science and Engineering*, 1st ed. London: CRC Press, 2022. doi: 10.1201/9781003164371.

[13] G. Plinius Secundus, *Storia naturale*, Rist., vol. II. Torino: Einaudi, 2005.

[14] C.-H. Lin, Y.-H. Yeh, Y.-I. Chen, J.-Y. Liu, and K.-J. Chen, "Earthquake Clustering Relative to Lunar Phases in Taiwan," *Terr. Atmos. Ocean. Sci.*, vol. 14, no. 3, p. 289, 2003, doi: 10.3319/TAO.2003.14.3.289(T).

[15] S. Kilston and L. Knopoff, "Lunar–solar periodicities of large earthquakes in southern California," *Nature*, vol. 304, no. 5921, pp. 21–25, Jul. 1983, doi: 10.1038/304021a0.

[16] M. Caputo and G. Sebastiani, "Time and space analysis of two earthquakes in the Appennines (Italy)," *NS*, vol. 03, no. 09, pp. 768–774, 2011, doi: 10.4236/ns.2011.39101.

[17] R. Z. Ren Zhenqiu, "河北大地震与朔望关系的剖析," *Chin. Sci. Bull.*, vol. 27, no. 10, pp. 617–620, May 1982, doi: 10.1360/csb1982-27-10-617.

[18] S. MAHMUD, *UNIQUE REASON OF EARTHQUAKE*. S.l.: LAP LAMBERT ACADEMIC PUBL, 2020.

[19] Ketkar, R, Viladkar, M. N.;, and Agrawal, P. N., "Study of Co-seismic Planetary Conditions for Earthquake Prediction"," *International Conferences on Recent Advances in Geotechnical*

Earthquake Engineering and Soil Dynamics. 15., 1991, [Online]. Available: https://scholarsmine.mst.edu/icrageesd/02icrageesd/session12/15
[20] Jeganathan, C., Gnanasekaran, G., and Tanushree Sengupta, "Analysing the Spatio-Temporal link between Earthquake Occurrences and Orbital Perturbations induced by Planetary Configuration," *International Journal of Advancements in Remote Sensing, GIS and Geography*, vol. 3, no. 2, pp. 123–146, 2015.
[21] A. Schuster, "On lunar and solar periodicities of earthquakes," *Proc. R. Soc. Lond.*, vol. 61, no. 369–377, pp. 455–465, Dec. 1897, doi: 10.1098/rspl.1897.0060.
[22] H. Hui and L. Xiaoming, "Research on Correlation of Positions of Celestial Objects with Earthquakes," *Natural Hazards*, vol. 23, no. 2/3, pp. 339–348, 2001, doi: 10.1023/A:1011115708096.
[23] L. Métivier, O. de Viron, C. P. Conrad, S. Renault, M. Diament, and G. Patau, "Evidence of earthquake triggering by the solid earth tides," *Earth and Planetary Science Letters*, vol. 278, no. 3–4, pp. 370–375, Feb. 2009, doi: 10.1016/j.epsl.2008.12.024.
[24] S. Ide, S. Yabe, and Y. Tanaka, "Earthquake potential revealed by tidal influence on earthquake size–frequency statistics," *Nature Geosci*, vol. 9, no. 11, pp. 834–837, Nov. 2016, doi: 10.1038/ngeo2796.
[25] T. H. Heaton, "Tidal Triggering of Earthquakes," *Geophysical Journal International*, vol. 43, no. 2, pp. 307–326, Nov. 1975, doi: 10.1111/j.1365-246X.1975.tb00637.x.
[26] Z.-Y. Ding, J.-K. Jia, and R. Wang, "Seismic triggering effect of tidal stress," *Tectonophysics*, vol. 93, no. 3–4, pp. 319–335, Apr. 1983, doi: 10.1016/0040-1951(83)90289-5.
[27] D. Zaccagnino, F. Vespe, and C. Doglioni, "Tidal modulation of plate motions," *Earth-Science Reviews*, vol. 205, p. 103179, Jun. 2020, doi: 10.1016/j.earscirev.2020.103179.
[28] A. Rovida, M. Locati, A. Antonucci, and R. Camassi, "Archivio Storico Macrosismico Italiano (ASMI)," p. 6000 earthquakes, 670 data sources, 30000 macroseismic intensity data points, Jun. 2017, doi: 10.13127/ASMI.
[29] P. Bretagnon and G. Francou, "VizieR Online Data Catalog: Planetary Solutions VSOP87 (Bretagnon+, 1988)," *VizieR Online Data Catalog*, p. VI/81, May 1995.
[30] I. Newton, *Philosophiæ naturalis principia mathematica*. in Early English Books Online / EEBO. Jussu Societatis Regiae ac Typis Josephi Streater. Prostat Venales apud Sam. Smith ad insigna Principis Walliae in Coemiterio D. Pauli, aliosq, nonnullos Bibliopolas, 1687. [Online]. Available: https://books.google.it/books?id=-3RXspUecy4C
[31] N. S. Mohamad and K. Chellappan, "The relationship between total electron content (TEC), tides phenomena and the position of moon and sun during the full moon and new moon in Selangor," in *2015 International Conference on Space Science and Communication (IconSpace)*, Langkawi, Malaysia: IEEE, Aug. 2015, pp. 277–282. doi: 10.1109/IconSpace.2015.7283766.
[32] Istituto Nazionale di Geofisica e Vulcanologia (INGV), "Rete Sismica Nazionale (RSN)," p. approx. 27 GB per day of new waveform data, approx. 415 active seismic stations, the archive totals to more than 600 distinct seismic stations, Dec. 2005, doi: 10.13127/SD/X0FXNH7QFY.

Declarations

Ethics approval and consent to participate

Not applicable

Consent for publication

Not applicable

List of abbreviations

FR → Resulting Gravitational Force exerted by the planet of the Solar System, the Moon and the Sun.

σFR → Standard Deviation of the Resulting Gravitational Force

Availability of data and materials
You can find data and materials in the Zenodo repository

Competing interests
The authors declare that they have no competing interests.

Funding
This study was not financially supported by any institution.

Authors' contributions
All authors read and approved the final manuscript.

Acknowledgements
We thank for the support to this Research, provided with numerous suggestions, especially: Carlo Doglioni (INGV President, Italy), Paolo Gasperini (Department of Physics, Geophysics Sector, University of Bologna), Luigi Cavaleri (ISMAR - CNR, Venice, Italy), Francesco Celani, (INFN, Frascati, Italy), Daniele Cataldi, LTPA Observer Project group.
We thank for meticulous checking of the text Roberto Pigro (MD, PhD Università degli Studi di Udine, Cipro).
Finally, we thank for supporting my public interventions the mathematician Claudio Pace (Terni, Italy).

LIST OF FIGURES AND TABLES

Graphical Abstract

Figure 1. Determination of angular distance in a spherical plane. The angular *value BD serves as the "angular distance",* summarizing the delta between the azimuths DC and the delta between the elevations BC of the 2 planets B and D relative to the Earth O observer. The equation $DB^2 = DC^2 + BC^2$ applicable to the Cartesian plane is adaptable to spherical planes, which are utilized when calculating sidereal distances. However, points B, C, and D lie *on different spherical planes* due to their construction, necessitating simplification if placed on a single spherical plane. The spherical right triangle Pythagorean Theorem converges to the Cartesian plane's classical Pythagorean Theorem when the sphere's radius $r \to \infty$, we use the Taylor polynomial 1-x2/2. *This allows us to simplify the "angular distance" from the spherical plane to the Cartesian plane for calculations.*

Figure 2. Vector calculation of the resultant gravitational force FR. a) Example of the sum of 2 vectors exerting equal force; b) Vector Newton forces of 2 planets and the Earth; c) Example of the sum of 3 vectors and their resultant force. We calculate the total of these vectors at any time by summing the FR (the resultant gravitational forces) of two celestial bodies, each multiplied by the cosine of the adjacent half-angle, *according to Carnot's theorem* (Figure 2,a). After placing on the abscissae the FR vector $\vec{b}$ (expressed in Newtons, henceforth "N") N(0) of Earth/Sun, with coordinates (b,0), the other vectors (n), with $n \in (2,9)$, have Cartesian coordinates $\vec{a}$(n) cos γ, a(n) sin γ, with $n \in (2,9)$ and constitute the N(n) force of one of the 9 planet/Earth combinations (figure 2,b). In the case of at least three forces, *the resultant gravitational force FR would be to be calculated according to the scheme in Figure 2,c.*

Figure 3. The cumulative percentile of Alert Time of the earthquake l'Aquila (Central Italy), 6.04.2009, M6.1. The value of parameter A (σ48hFR) with Index 5 is 4.5607E-11. The value of parameter B (σ24hFR) with Index 1 is 7,96239E-09. The percentile of the Alert Time in 1 month is 6%.

Figure 4. Distribution of average number of alignments <12° by magnitude range of earthquakes occurring after 1988. Average number of alignments <12° for each magnitude range (Richter), with the Moon (left graph) and without (right graph) at the triggering time of both the 200 earthquakes since 1600 and the 63 earthquakes that occurred after 1988. *The average number of alignments rises as the magnitude increases.*

Figure 5. Distribution of average angular distance <12° by magnitude range of the 200 earthquakes. Average angular distance <12° for each magnitude range (Richter), with the Moon (left) and without (right graph) at the triggering time of both the 200 earthquakes since 1600 and the 63 earthquakes that occurred after 1988. *The average angular distance of alignments decreases as the magnitude increases.*

Figure 6. Normal distribution of average angular distances <12° at the trigger time of the 200 earthquakes. The distribution of the 200 average angular distances <12° at the time of seismic triggering (with the Sun and the Moon on the left, without the Moon on the right) is validated with a 95% confidence interval using the *Shapiro-Wilks and P-value tests*, *with a p-value of 0.1531 (left graph).* Interestingly, the average angular distances calculated including the Moon along with the seven planets and the Sun showed a better fit to a normal distribution compared to the same calculations excluding the Moon, that shows *a p-value of 0,0675 (right graph)*. The p-value for the distribution of average angular values including the Sun and Moon of the sample of 63 earthquakes that occurred after 1988 is 0.0506. While the p-value excluding the Moon from the calculation is 0.1542 (see Table 6). *The normality of all distributions in this section was then validated with a p-value >0.05.*

Figure 7. Polynomial distribution of the % Alert Time, without Sun-Moon (Analysis Line 3). Notably, the most reliable distribution for identifying seismic trigger Alert Times for all 200 earthquakes is *the formula describing the distribution of percentile Alert Time* influenced by σFR during triggering within 1 month, *found in Analysis Line 3*: $\boldsymbol{Y = 6.04-411x+10477x^2-48042x^3+95878x^4-72550x^5-27113x^6+71599x^7-29759x^8}$ (See Table 8 for details). This particular polynomial distribution boasts an *impressive regression coefficient R^2 of 0.999, the closest value to 1 in the entire study.* This result holds true when compared to the R^2 values of the other two Analysis Lines (see *infra*, Figure 8).

Figure 8. Summary/comparative table of the R^2 regression coefficients of the 3 parameters identifying σFR. This table presents a summary and comparison of the regression R^2 coefficients for the three σFR indices (parameters A, B, and % Alert Time) for both the 200 earthquakes (on the left) and the 63 earthquakes occurring after 1988 (on the right) across the three lines of analysis. Notably, the regression coefficient R^2 of 0.999 in Analysis Line No. 3 (on the left) is the closest value to 1 in the entire case study. Similarly, the right graph, representing the R^2 regression coefficients for the 63 earthquakes occurring after 1988, yields results very similar to those on the left, indicating once again that *Analysis Line No. 3 exhibits values closest to 1*, than the other two, even for the most recent sample of earthquakes.

Figure 9. Distribution of σFR indices of parameter A (left graph) and of parameter B (right graph). This figure presents a summary of the distribution and a comparison of σFR indices between

the sample of 200 earthquakes and the sample of 63 earthquakes within the reference month for both parameter A (Left) and parameter B (Right). Following the line of analysis No. 2 graphs show that both distributions have a *median value (parameter A) of 3* and 95% of the earthquakes are concentrated within a low σFR index value of 9 (the maximum possible σFR index value is 14, see *supra*, Section 2.9.1); For the other σFR index (parameter B), however, both distributions have *a median value of 5*, and 95% of the earthquakes are concentrated within a consistently low σFR index value of 24-25 (the maximum possible σFR index value is 347, see *supra*, Section 2.9.2). As explained, index 1 corresponds to the highest or lowest σFR value of the month, index 2 to the second highest or lowest value, and so on. For the remaining lines of analysis, specifically No. 1 and 3, *the data concentration shows a striking similarity for both the 200 earthquakes since 1600 and the 63 earthquakes that occurred after 1988*. Refer to Table 8 for details.

Figure 10. Pareto plot of the percentile Alert time over a month. This figure presents a summary and comparison of the σFR % Alert Time for both the 200 earthquakes (on the left) and the 63 earthquakes occurring after 1988 (on the right) for the reference month. Following the line of analysis No. 1 graphs show that both distributions have a median % Alert Time value of 17-18%. Besides, *95% of the earthquakes are concentrated within a narrow % Alert Time of 56-68%*. For the remaining lines of analysis, specifically No. 2 and 3*, the data distribution (Pareto plots and histograms) also shows a striking similarity* for both the 200 earthquakes since 1600 and the 63 earthquakes that occurred after 1988: refer to Table 8 for details.

Figure 11. Chart of the gravitational and tidal force per mass Earth unit at the perigee. This is a comparative table of the tidal and gravitational forces exerted by celestial bodies in the Solar System at perigee. These insights emphasize the significant differences in gravitational and tidal components between celestial bodies in the Solar System.

Table 1 DOI 10.5281/zenodo.7746082, VSOP87 - Celestial Sphere - Delta Mask and Software, for Section 2.6

Table 2 DOI 10.5281/zenodo.7734562, VSOP87 - Celestial Sphere - Delta Mask and Software, for Section 2.8.

Table 3 DOI 10.5281/zenodo.7779003, Study of FR gravitational forces exerted by the angular distances of all 9 S.S. celestial bodies toward Earth: L'Aquila Earthquake, 06.04.2009, Italy, M6.1, for Section 2.9.

Table 4 DOI 10.5281/zenodo.8171569, APPENDIX – List of earthquakes, for Section 2.9.

Table 5 DOI 10.5281/zenodo.8083305, Random sample extraction of 145 earthquakes, for Section 2.10.1.

Table 6 DOI 10.5281/zenodo.10058522, Summary Excel tables of results of the first hypothesis, for both the sample of 200 earthquakes since 1600 and the 63 earthquakes that occurred after 1988, for Section 3.1.

Table 7 DOI 10.5281/zenodo.10058668, **Summary graphs of the data distributions of the** Hypothesis 2**, with the R^2 regression values** of the three σFR values and indices (parameters A, B and % Alert Time) of both the 200 earthquakes and the 63 earthquakes after 1988, for Section 3.2.

Table 8 DOI 10.5281/zenodo.10058786, **Summary distribution and probability** of the three σFR indices (parameters A, B and % Alert Time) **of the** Hypothesis 2 for both the 200 earthquakes and the sample of 63 earthquakes after 1988, for the three lines of Analysis.

Table 9 DOI 10.5281/zenodo.10061252, **Overview of the 200 analyzed earthquakes encompassing values and indices for σFR Parameters A, B, and the percentile of Alert Time across the three Analysis Lines.**

Table 10 DOI 10.5281/zenodo.8163189, **Overview and details of the 200 analyzed earthquakes encompassing values and indices for σFR Parameters A, B, and the percentile of Alert Time across the three Analysis Lines.**